

Evaluation of coated metallic bipolar plates for polymer electrolyte membrane fuel cells

Wonseok Yoon^a, Xinyu Huang^{a,*}, Paul Fazzino^a, Kenneth L. Reifsnider^a,
Michael A. Akkaoui^b

^a *University of Connecticut, Connecticut Global Fuel Cell Center, 44 Weaver Road, Unit 5233 Storrs, CT 06269-5233, USA*

^b *Tanury Industries, 6 New England Way, Lincoln, RI 02865, USA*

Received 24 November 2007; received in revised form 5 December 2007; accepted 5 December 2007

Available online 23 December 2007

Abstract

Metallic bipolar plates for polymer electrolyte membrane (PEM) fuel cells typically require coatings for corrosion protection. Other requirements for the corrosion protective coatings include low electrical contact resistance, good mechanical robustness, low material and fabrication cost. The authors have evaluated a number of protective coatings deposited on stainless steel substrates by electroplating and physical vapor deposition (PVD) methods. The coatings are screened with an electrochemical polarization test for corrosion resistance; then the contact resistance test was performed on selected coatings. The coating investigated include Gold with various thicknesses (2 nm, 10 nm, and 1 μm), Titanium, Zirconium, Zirconium Nitride (ZrN), Zirconium Niobium (ZrNb), and Zirconium Nitride with a Gold top layer (ZrNAu). The substrates include three types of stainless steel: 304, 310, and 316. The results show that Zr-coated samples satisfy the DOE target for corrosion resistance at both anode and cathode sides in typical PEM fuel cell environments in the short-term, but they do not meet the DOE contact resistance goal. Very thin gold coating (2 nm) can significantly decrease the electrical contact resistance, however a relatively thick gold coating (>10 nm) with our deposition method is necessary for adequate corrosion resistance, particularly for the cathode side of the bipolar plate.

© 2008 Published by Elsevier B.V.

Keywords: Fuel cells; Metallic bipolar plates; Coating; Corrosion; PVD

1. Introduction

The bipolar plates for the polymer electrolyte membrane fuel cell (PEMFC) perform multiple functions, such as conducting electrons between adjacent cells, separating and distributing fuel and oxidant, and carrying away reaction products and heat from each cell. In order to perform these functions well, bipolar plates need to have low contact resistance and high electrical conductivity, high thermal conductivity, low gas permeability, good mechanical strength, satisfactory corrosion resistance, or suitable surface properties for liquid water removal. Traditionally, graphite and graphite composite plates with machined flow fields have been widely used in PEMFC because of their high corrosion

resistance, and low interfacial contact resistance (ICR). However, their poor manufacturability results in high fabrication cost, and their brittleness requires the use of fairly thick plates for adequate mechanical strength. Recently, metallic bipolar plates have received much attention as an alternative bipolar plate material because of their superior mechanical strength, low gas impermeability, very high bulk electrical and thermal conductivity, relatively low material and manufacturing cost [1]. Typically, bipolar plates are exposed to a warm (65–90 °C), acidic (pH 2–3) and humid environment. Under such conditions, the thermodynamically stable state of most of the metallic elements is frequently the cations, rather than the metal itself. For example, in the case of stainless steel bipolar plates, metal cations, such as Fe^{2+} , Ni^{2+} and Cr^{3+} can be released during the corrosion process [2]. Additionally, poorly conductive metal oxides can form on the corroded surfaces, increasing the ICR of the contacting surfaces and thus reducing fuel cell performance.

The corrosion process is an electrochemical process which involves both oxidation and reduction reactions. In case of metal

* Corresponding author. Present address: Florida Solar Energy Center, University of Central Florida, 1679 Clearlake Road, Cocoa, FL 32922-5703, USA. Tel.: +1 321 638 1706; fax: +1 321 638 1010.

E-mail address: xhuang@fsec.ucf.edu (X. Huang).

corrosion in acid solution, metal oxidation takes place at the anode sites, and reduction of hydrogen ions occurs at cathode sites [3–5]. The processes can be represented as follows:



In Eq. (1), M represents surface metal element, M^{n+} is the corresponding metal ion in the solution, e^{-} is free electron; in Eq. (2), H^{+} and H_2 represent proton adsorbed on metal surface and the evolved hydrogen gas. Besides these, oxidation and reduction reactions involving other ions (ferrous and hydroxide ions) and species (oxygen) can also occur depending on the solution used.

The corrosion reactions involve the transfer of electrons and ions between the metal and the solution. Without an external applied potential or external source of electrons, surface corrosion reactions normally occur at a potential for which the rate of oxidation and reduction are electrochemically balanced. The equilibrium potential (corrosion potential, E_{CORR}) and the associated current (corrosion current, I_{CORR}) can be measured by an electrochemical polarization test. E_{CORR} and I_{CORR} are widely used as the indicators of the corrosion resistance of a material. A typical polarization curve for bare stainless steel (316) is shown in Fig. 1. The corrosion current and corrosion potential are determined by extrapolating the tangential line of the anodic and cathodic polarization curve.

Comprehensive research has been conducted on metallic bipolar plates and protective coatings over the past few years. An Fe-based alloy (FeB) and Ni-based alloy (NiB) were investigated for the suitability of cost-effective bipolar plates [6]. The polarization characteristics of the fuel cells with FeB plates tested indicated that most of the FeBs exhibited a characteristic behavior comparable to that of the Ni-based alloy (NiB) and was found to be susceptible to pitting corrosion. Moreover, contact resistance was about $100 \text{ m}\Omega \text{ cm}^2$ at 140 N cm^{-2} , which was higher than that of NiB and does not meet the DOE targets (Table 1 [7]). Fleury et al. [8] evaluated an Fe-based amorphous alloy for the bipolar plates; the contact resistance of the Fe-based amorphous alloys were found to be similar to that of stainless steel and their

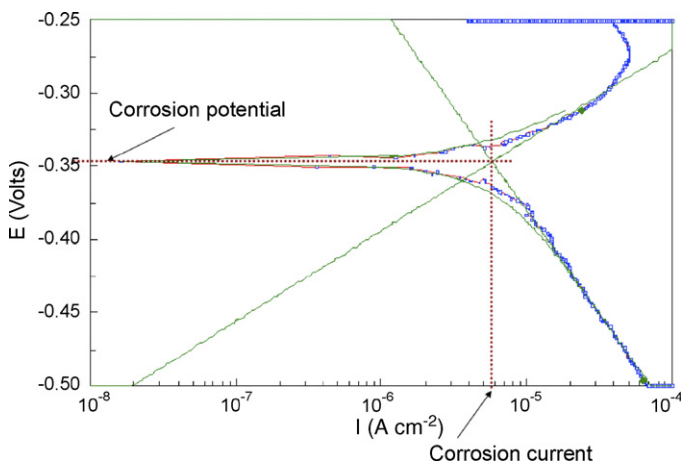


Fig. 1. Polarization curve of bare SS 316 around the corrosion potential in pH 2 H_2SO_4 solution at 80°C (Potential vs. SCE).

Table 1
DOE targets for 2010; ICR, corrosion resistance, and cost

| Performance metrics | DOE goal by 2010 |
|---|------------------|
| ICR at 140 N cm^{-2} ($\text{m}\Omega \text{ cm}^2$) | 10 |
| Corrosion current at $-0.1 \text{ V (H}_2)$ ($\mu\text{A cm}^{-2}$) | <1 |
| Corrosion current at 0.6 V (air) ($\mu\text{A cm}^{-2}$) | <1 |
| Cost ($\text{\$ kW}^{-1}$) | 6 |

corrosion resistance was poor in comparison with the graphite plates.

Stainless steel (SS) is the most widely used candidate for metallic bipolar plates and numerous reports have been published on this material by several institutes and universities over recent years. Stainless steel's relatively high resistance to corrosion, relatively low cost, and superior manufacturability make it an ideal base material for a host of commercial applications. Makkus et al. [9] conducted fuel cell testing with different stainless steel bipolar plates. The results show a current decay of approximately 30–50% in the first 300 h of operation, and a high metal ion concentration in the MEA. Similar work was performed by Davies et al. [10] with 310, 316 and 904L stainless steel bipolar plates. Li et al. [11] examined the corrosion behavior of 316 SS in a simulated anode environment. They stated that a coating needs to be developed to enhance the corrosion resistance of the stainless steel.

Some researchers investigated gold-coated bipolar plates, since gold, itself, is the one of the best corrosion resistance materials and an excellent electrical conductor. Hentall et al. [12] and Woodman et al. [13] fabricated current collectors from aluminum, then coated them with gold by a solution process. It was found that the fuel cell data with gold-coated bipolar plates showed a comparable performance to that of cells with graphite plates.

Wang et al. [14] conducted short-term fuel cell performance testing with gold-plated titanium bipolar plates. Since a long-term corrosion test was not implemented, feasibility of the bipolar plate was not completely validated. Surface contact resistance below $1 \text{ m}\Omega$ was measured at a compaction torque in the range from 20 kgf cm to 60 kgf cm . Cell polarization curves indicated that the cell performance with coated plate was quite similar to that of graphite plates. Their cell was tested at 40°C with 5 psi back pressure; the humidification temperature of anode and cathode, 90°C and 80°C , respectively.

Most coatings for metallic bipolar plates have been proven inadequate due to pin-hole defects, which cause local corrosion and metallic ion contamination of the membrane. Recently, nitridation has been identified as an alternative coating method for metallic bipolar plates due to the combination of high electrical conductivity and good corrosion resistance [15]. The nitride layer is formed by nitrogen atom penetration and diffusion into the substrate, for which there is less interfacial adhesion problem, and is characterized by high corrosion resistance [16].

Brady et al. [15] have recently developed a preferential thermal nitridation process to generate a pinhole-free coating on a Ni–Cr alloy base plate, which shows excellent corrosion resis-

tance and negligible contact resistance. Nitrided surface showed a significantly lower contact resistance than that of 316L SS. In addition, a single cell test (operated at a constant voltage of 0.7 V) data indicated trace levels of Ni and Cr in the range of 0.01–0.3 $\mu\text{g cm}^{-2}$ over a 1000-h test period.

Feasibility of thermally nitrided stainless steel was also studied by Wang et al. [16]. A 2-h and a 24-h nitridation treatment were developed for the AISI446 SS. Cell polarization data showed that the 2-h nitrided AISI446 exhibited better corrosion resistance and smaller ICR than the 24-h nitrided AISI446. They pointed out that the nitrided layer developed on 24-h nitrided AISI446 was not continuous, which resulted in poor corrosion resistance. The 2-h nitridation treatment created a nitrogen modification of the native passive oxide layer on the alloy, which improved corrosion resistance in the simulated PEMFC environments. However, the ICR value, 40 $\text{m}\Omega \text{cm}^2$ at 150 N cm^{-2} after polarization test, did not meet the DOE targets.

Rujin Tian et al. [17] examined the corrosion behavior of plasma-nitrided austenitic 316L SS bipolar plates and Li et al. [18] investigated the corrosion behavior of TiN-coated 316 SS in a simulated PEMFC environment. The authors concluded that TiN-coated 316 SS has higher corrosion resistance and surface conductivity than uncoated 316 SS with no significant effect on TiN coatings under the typical load conditions for 4 h. However, further study is needed to improve the coating quality and to evaluate the long-term stability of TiN coating. Cho et al. [19] also developed TiN-coated bipolar plate, which significantly improved the initial performance and lifetime when compared to 316 SS; however, the performance is still lower than that of graphite.

To date, feasibility of various protective coating materials and coating methods for metallic bipolar plates has been investigated and some of them showed promising results in mostly short-term tests. However, for commercial automotive application of the metallic bipolar plates, an operation time over 5000 h without significant performance degradation has to be guaranteed. As such, long-term corrosion and fuel cell testing are necessary for evaluating coating materials for metallic bipolar plates. Our research on coated metallic bipolar plates is structured into three phases: Phase I includes mostly short-term screening tests such as polarization and contact resistance tests; in Phase II, long-term corrosion test using a corrosion test cell will be carried out; in Phase III mid-term and long-term fuel cell testing will be conducted to further evaluate selected coatings on metal bipolar plates. This paper reports the results of our Phase I work for a set of coating materials. Mid-term and long-term test results will be reported in subsequent papers.

2. Experimental

2.1. Sample preparation

For this research, austenitic stainless steel 304, 310, and 316 were used for substrate material since they were known to be corrosion resistant materials in many other applications. The first subset of coating materials are listed in Table 2. The substrates and coated samples were obtained from Tanury Industries Inc.

Table 2
Substrates and coating materials

| Substrate | Coating materials | | |
|-----------|---|---|-------------------------|
| SS 304 | 2 nm gold, 10 nm | Zr, ZrN, ZrNb, | Ti (0.5 μm) |
| SS 310 | gold, 1 μm gold ^a | ZrNAu ^b (0.5 μm) | |
| SS 316 | | | |

^a Coated on SS 316 only.

^b 10 nm gold thickness.

Coating was deposited on as-fabricated substrates without any surface grinding or polishing.

For the deposition of coatings, both high speed acid gold plating and two methods of physical vapor deposition were employed. For gold only coatings, the electroplating process was used. Tanury used a high speed gold plating chemistry where the cathode film was rapidly changed or recharged with gold. This process allowed for very uniform thin deposits in relatively short periods of time, hence reduced material and fabrication cost. For all other samples that used titanium, zirconium, or niobium, the samples were coated using either magnetron sputtering or cathodic arc coating systems. In both of these PVD processes, the samples are placed into a vacuum chamber and pumped down to 10^{-5} Torr or 10^{-6} Torr to create an environment that is contaminant free and will allow a free flow of plasma gases. At a preset vacuum, argon gas is fed into the chamber via mass flow controllers. The pressure of the system is monitored and controlled as the argon is fed in to the chamber. The argon gas is energized creating a glow discharge etch process inside the chamber resulting in a cleaner and active surface for deposition of the initial layer. Once this stage is complete, high negative potential is applied to the substrate while the target material is energized at low power. Coating material is attracted to the negatively charged substrate and forms a bond. Due to the high negative potential applied to the substrate, particles that do not adhere are intentionally ejected from the substrate and are replaced by those that have bonded resulting in a firm bond between the substrate and the new coating. Once this phase is complete, the system is programmed to grow a film of the target material by combining these ions with reactive gases. The type of reactive gas used results in the type of compound that is grown on the substrate surface. For instance, when making a zirconium nitride, we introduce a controlled amount of nitrogen gas with the proper proportion of argon during the zirconium PVD process. Similarly, to produce carbides coating, we utilize methane or acetylene as the reactive gas. Once the thin film layer is built to the target thickness, the chamber is vented and the samples are removed.

2.2. Short-term corrosion test

The corrosion property of a material was characterized by the polarization test. A commercially available electrochemical corrosion test cell was employed to conduct the polarization test, as illustrated in Fig. 2. The components of the corrosion cell include the metal sample as the working electrode (WE), a reference electrode (RE, SCE), a counter electrode (CE, Graphite

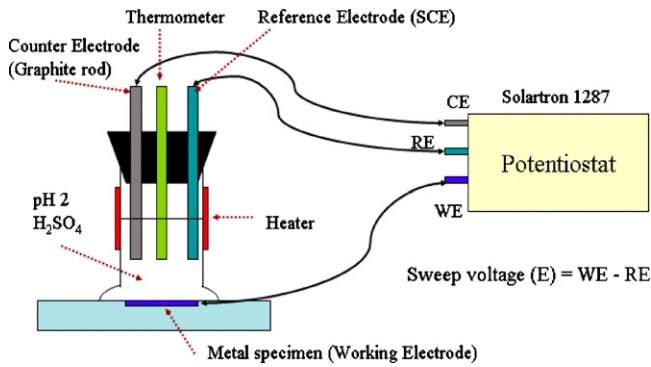


Fig. 2. Experimental setup for polarization test.

rod). A potentiostat (Solartron 1287) was used to control the relative potential of the metal sample (WE) with respect to the reference electrode (RE). A plot of potential vs. current is called a polarization curve as presented in Fig. 1.

In the polarization test, the potential of the metal coupon was changed from negative 1 V to positive 1 V at a 1 mV s^{-1} scan rate. The corrosion bath used was an aqueous H_2SO_4 (pH 2) solution and the temperature of the solution was maintained at 80°C using an external heater around the cell; these conditions are representative of an operating PEMFC. Before the test, all samples were degreased and rinsed with DI water. Corrosion surface area is 3 cm^2 and a polarization test for each sample was conducted after a 1 h dwell in the solution for the redox reaction to be stabilized [11]. Fresh corrosion bath was used for each new sample.

2.3. Contact resistance test

In PEMFC, bipolar plates are typically in contact with gas diffusion layers such as carbon paper or carbon cloth. Interfacial contact resistance should be minimized for better fuel cell efficiency. Interfacial contact resistance tests were conducted for selected coated samples to pick the best candidate for Phase II

long-term corrosion test and actual fuel cell testing. For comparison purposes, a bare SS 316 and a graphite plate were also tested. Measurement techniques for interfacial contact resistance are well documented in the literature [10,20,21]. The measurement scheme is described as follows. As illustrated in Fig. 3, the sample (bare or coated on both sides) for contact resistance measurement is positioned between two pieces of carbon papers (Toray TGPH-120, 30 wt% wet proof), a typical gas diffusion medium in PEMFC. The carbon papers are pressed against the sample by a pair of gold-plated metal current collector plates. In order to apply a controlled uniform contact pressure between the metal sample and the carbon paper, a thick metal platen is pressed on to the sample assembly by a pneumatic cylinder. The top metal plate is connected to the actuator of the pneumatic cylinder via a universal joint to minimize bending moment. A precision regulator is used to control and maintain a constant pressure in the cylinder, hence the total compressive (or compact) force on the assembly.

To measure the resistance, some researchers apply a 1 A DC current through the metal plates and measure the voltage drop across them to calculate the contact resistance as a function of pressure. However, excessive current through the contacts during testing may cause a physical change in the contact area at the microscopic level. For example, high current may cause localized heating, which can soften or melt the contact points and the surrounding area [22,23]. To avoid such potential issues, a total current of less than 20 mA was applied to an area of approximately 13 cm^2 , the so-called dry circuit method [23]. In our experiment, an Agilent 4338B milliohm-meter (10 micro Ohm resolution) was employed for direct measurement of the total ohmic resistance. The meter supplied an AC current (1 kHz) ranging from $1 \mu\text{A}$ to 10 mA according to the magnitude of the target resistance. Before measurement, all of the samples were degreased and rinsed with DI water and all measurements were made at a room temperature. The measured total resistance (R_1) consisted of material's bulk resistance (R_b), lead resistance (R_{circuit}), and interfacial resistances from four con-

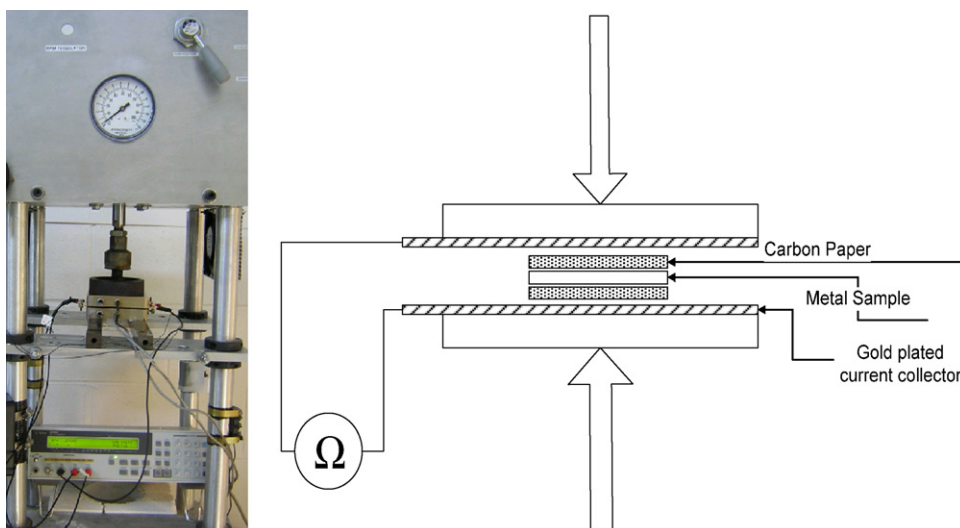


Fig. 3. A picture (left) and a schematic of the interfacial contact resistance measurement setup.

tact pairs, which included two contact pairs of carbon paper and gold-plated current collector and two contact pairs of carbon paper and the bare or coated (on both sides) metal bipolar plate sample under investigation. It is believed that the bulk resistances of the metallic components were negligible compared to the interfacial contact resistance. What we wanted to measure was the contact resistance between the carbon paper and the metal sample. Therefore, a calibration test was performed by measuring the resistance (R_2) of only one carbon paper placed in between the gold plated current collectors without the metal sample, and subtracting that value from the total resistance (R_1) measured with the metal sample in place. The contact resistance of the metal sample can be calculated by the following equation. The area specific contact resistance $^1(\Omega \text{ cm}^2)$ is obtained by multiply the measured contact resistance R_{ct} (Ω) with the contact area (cm^2) of the specimen.

$$R_1 = 2R_{ct} + 2R_{C-G} + R_{circuit} + R_{b1} + R_{b2} \quad (3)$$

$$R_2 = 2R_{C-G} + R_{circuit} + R_{b2} \quad (4)$$

$$R_{ct} = \left(\frac{R_1 - R_2}{2} \right) \quad (5)$$

where R_1 is the total resistance with metal sample (Ω), R_2 the total resistance without metal sample (Ω), R_{C-G} the Contact resistance between the carbon paper and gold-coated current collector (Ω), $R_{circuit}$ is the Ohmic resistance of the leads in the measurement circuit (Ω).

3. Results and discussion

3.1. Polarization test results

Corrosion potential and corrosion current can be estimated from the polarization test result of each sample. They are approximate indicators for the corrosion resistance of the materials. A higher corrosion potential and lower corrosion current usually indicate a higher corrosion resistance.

Fig. 4 shows the polarization curves of three types of bare SS samples. It can be seen that they behave very similarly in this test. The corrosion potential (-0.347 V vs. SCE) of SS 316 is slightly higher than other two samples. All three samples showed a passivation behavior in the potential range from -0.2 V to 0.6 V (*vs. SCE*).

Fig. 5 shows the polarization curve of the three types of SS coated with 2 nm gold. It shows that the 2 nm gold coating does not produce a discernable effect on the corrosion characteristics of the metal substrates except for increasing the corrosion potential slightly by about 50 mV.

Fig. 6 shows the polarization test results of the three SS coated with 10 nm gold. The 10 nm gold coating was found to improve the corrosion resistance remarkably by increasing the corrosion potential and decreasing the corrosion current regardless of what type of substrates were used. The corrosion potential of all samples was increased up to approximately 0 V with respect to SCE

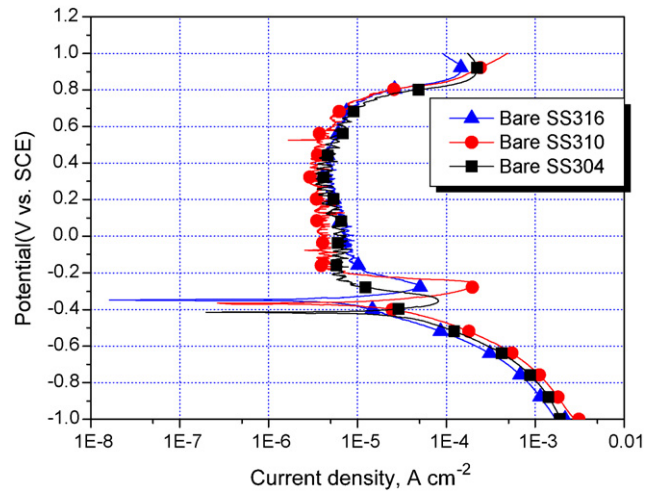


Fig. 4. Polarization curve of bare SS 304, 310, and 316 samples.

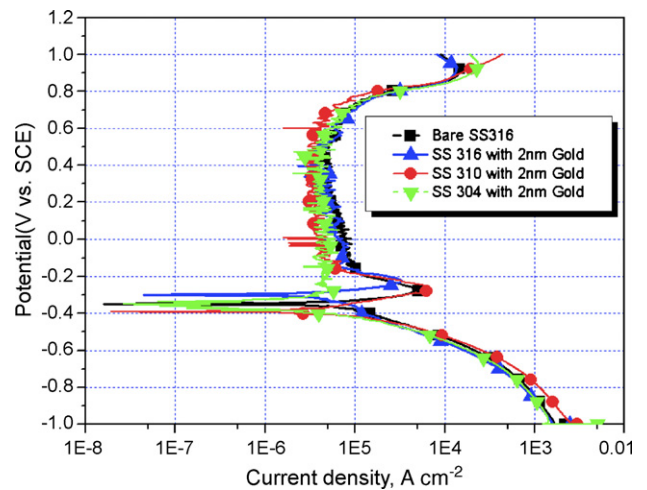


Fig. 5. Polarization curve of SS 304, 310, and 316 with 2 nm gold coating.

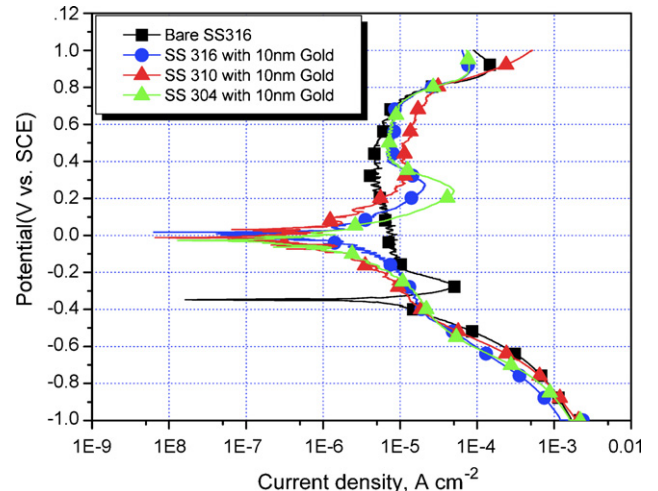


Fig. 6. Polarization curve of bare SS 304, 310, and 316 with 10 nm gold coating.

¹ Neglect R_{b1} and R_{b2} , bulk resistance of metal samples and carbon papers.

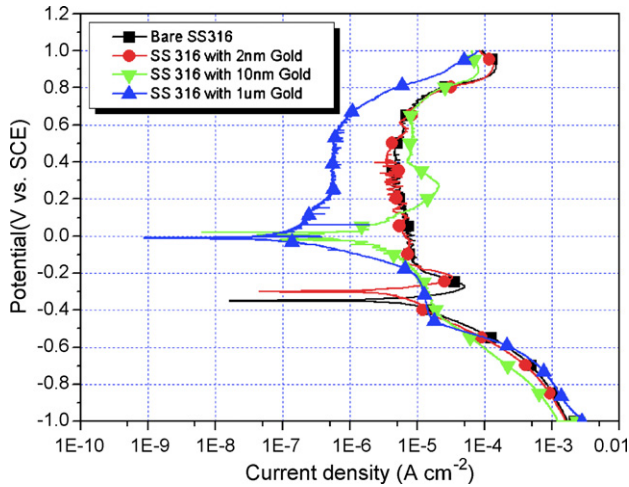


Fig. 7. Gold thickness effect on the corrosion resistance of SS 316.

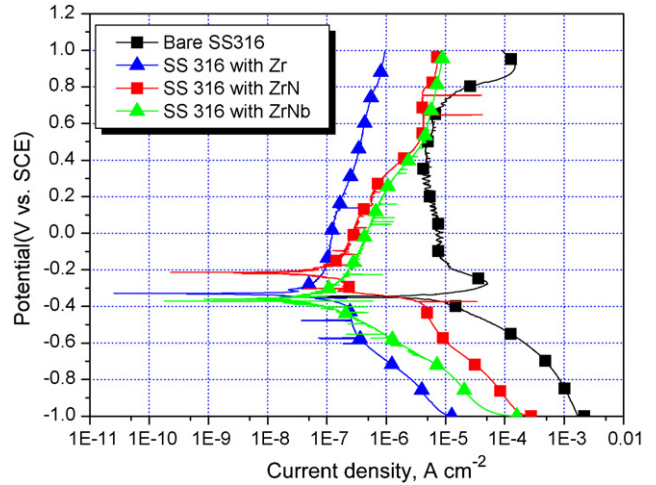


Fig. 9. Polarization test of Zr, ZrN and ZrNb coating on the SS 316 sample.

and the corrosion current density (e.g. 5.6568 $\mu\text{A cm}^{-2}$ for SS 316) was less than $1 \mu\text{A cm}^{-2}$, which is the DOE target for a corrosion test. The passivation behavior can still be observed at a higher potential range.

To observe the effects of gold coating thickness on the polarization behavior, we further tested SS 316 samples with 1 μm thick gold coatings. The results are shown in Fig. 7. Compared to the 10 nm gold coating, one micron gold coating further reduces corrosion current. The thicker the gold coating is, the better corrosion resistance can be achieved particularly at higher potential ranges.

During the experiment, it was noticed that the corrosion behavior of different substrates with the same coating materials did not show much difference from each other, or that the SS 316 samples showed slightly better corrosion resistance than the others. It can be observed in the polarization curve of the gold-coated samples and Ti-coated samples in Fig. 8 as well. Because of that, only coated SS 316 samples were studied in subsequent testing. As shown in Fig. 9, the polarization curves of Zr, ZrN as well as ZrNb-coated SS 316 samples were obtained. It was found that the corrosion current of the Zr sample is the least among the this group and that ZrN and ZrNb exhibited better

corrosion resistance than bare SS 316 in terms of the corrosion current.

As noticed in Fig. 10, the 10 nm gold on the ZrN sample (ZrNAu) further enhanced the corrosion resistance of the ZrN sample in terms of the corrosion potential as well. In other words, it appears that the 10 nm gold coating is adequate for increasing the corrosion potential of the target substrates; however, the 10 nm gold on ZrN does not reduce the corrosion apparent current. Instead, 10 nm gold on ZrN raises the current at the low potential range.

The corrosion potential and current of all the samples with SS 316 substrate with different coating materials are summarized in Fig. 11. In a PEM fuel cell, the bipolar plate is positioned between an anode electrode where the hydrogen fuel is oxidized and a cathode electrode where the oxygen is reduced. The typical potential of the bipolar plate surface in contact with the anode electrode is approximately -0.1 V vs. SCE , and that of the bipolar plate surface in contact with the cathode electrode is 0.6 V vs. SCE [20]. As can be seen in Table 1, the current density less than $1 \mu\text{A cm}^{-2}$ in the potential range of approxi-

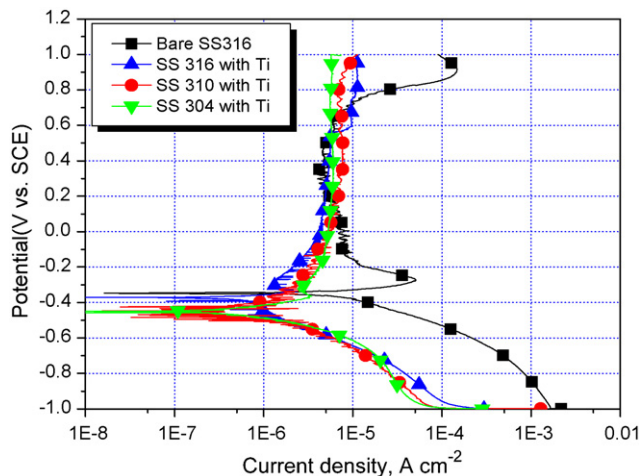


Fig. 8. Polarization curve of the bare SS 304, 310, and 316 with Ti coating.

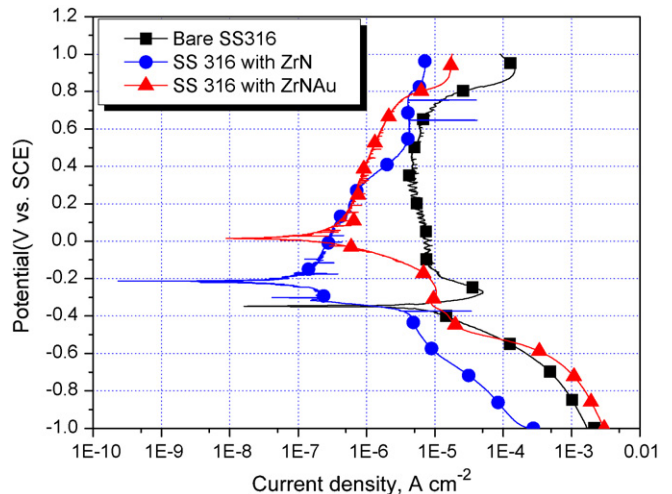


Fig. 10. Comparison of the corrosion resistance for ZrN and ZrNAu-coated SS 316 samples.

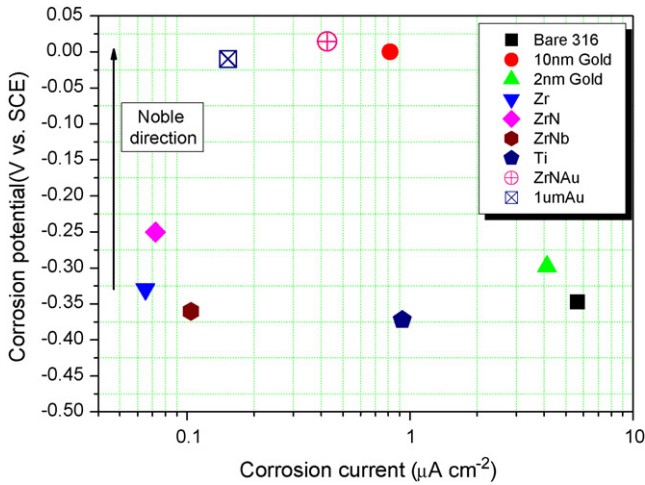


Fig. 11. Corrosion potential and current plot of SS 316 substrate sample with different coating materials in 0.01 N H₂SO₄ (pH 2) solution at 80 °C. The scan rate is 1 mV s⁻¹.

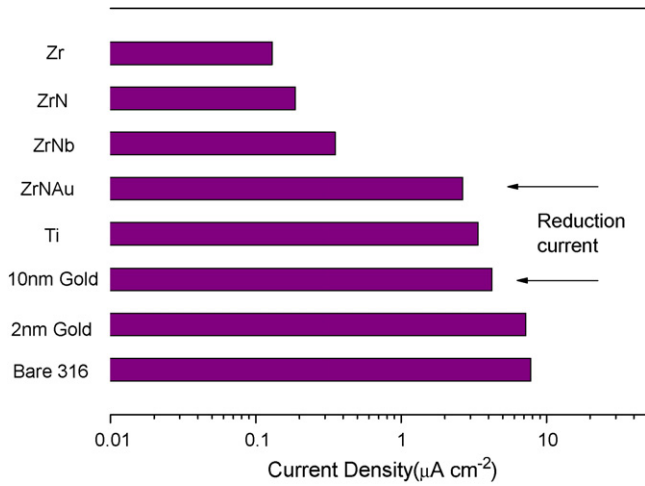


Fig. 12. Dissolution rate for metal samples at anode potential (-0.1 V vs. SCE).

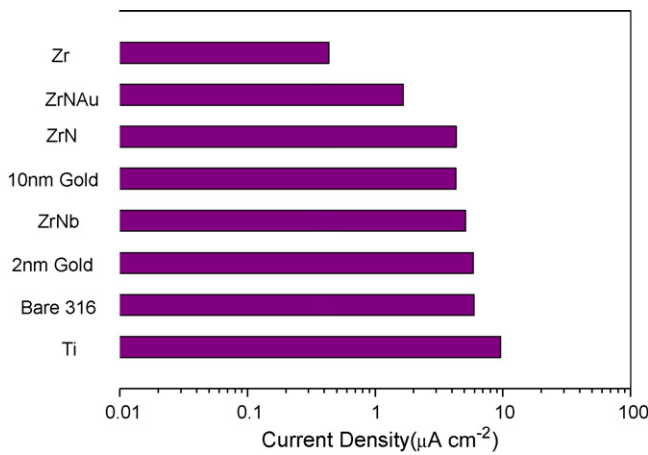


Fig. 13. Dissolution rate for metal samples at cathode potential (0.6 V vs. SCE).

mately -0.1 V to 0.6 V vs. SCE was recommended by DOE as a necessary requirements for PEMFC bipolar plate material.

Figs. 12 and 13 show the current density of metal samples at typical anode potential and cathode potential, respectively, in

fuel cell application. The data are extracted from above polarization test results. In the case of ZrNAu and 10 nm gold at anode potential shown in Fig. 12, the apparent current density may not totally attributed to the metal oxidation. Part of the apparent current may be due to the reduction current of oxygen [24], since -0.1 V is below the corrosion potential of two metal samples. Based on our test results, only Zr-coated samples satisfied the corrosion current density requirement of DOE at both anode and cathode potentials.

Since iron is a major constituent of the SS bipolar plates and less noble than other alloying elements and the coating materials, it is suspected that iron dissolution is one of the major anodic processes. According to Eq. (1), the amount of iron dissolved into the corrosion bath should be correlated to the total anodic polarization current. In order to confirm such a correlation, the concentration of iron cations in the corrosion bath of SS 316, SS 316 with 10 nm Au, and SS 316 with Zr samples were analyzed using an atomic absorption (AA) spectroscopy technique after the polarization test. Assuming that the total anodic current is attributed to the iron (Fe²⁺) dissolution (neglect other element, i.e., Cr, Ni, Mo, etc.), then a quantitative comparison can be made between a measured iron concentration in solution and predicted iron concentration based on the total electron charge of anodic processes via Faraday's law. Total anodic electron charge is obtained by integration of anodic current in the polarization curve. Table 3 and Fig. 14 show the comparisons of measured iron concentration and iron concentration estimated from the total anodic charge based on Faraday's law. The AA technique cannot distinguish different oxidation state of iron, i.e., Fe²⁺ or Fe³⁺. Therefore, it will detect all cation forms of the iron presented in the solution, which may be a source of error for this analysis. It can be observed that the iron concentration in the solution correlates very well with the total anodic charge. The iron dissolved in the corrosion bath can account for more than half of the total anodic charge. In the case of Zr-coated samples, the anodic current density is relatively low (1E-7 A cm⁻²) and the results may be affected by errors in the measurement of low currents.

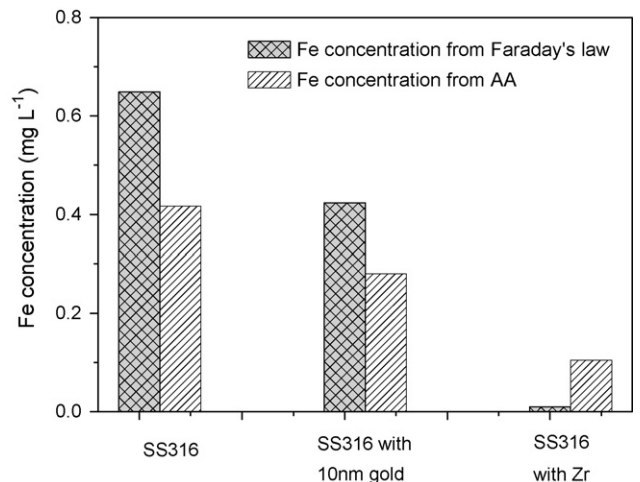


Fig. 14. Comparison of iron concentrations in solution of SS 316, SS 316 with 10 nm gold, and SS 316 with Zr samples after the polarization test.

Table 3
Estimation of iron dissolution from anodic current density

| Samples | Charge density (C cm ⁻²) | Mass consumption (g) | Conversion (from g to mg L ⁻¹) | Fe ²⁺ concentration by AA (mg L ⁻¹) | Remarks |
|-------------------|--------------------------------------|----------------------|--|--|--|
| 316 | 0.0299 | 1.7306E-5 | 0.6489 | 0.416 | Solution volume: 40 mL Fe molecular weight: 55.845 g mol ⁻¹ |
| 316 with 10 nm Au | 0.01953 | 1.1303E-5 | 0.4238 | 0.28 | |
| 316 with Zr | 4.34E-4 | 2.5142E-7 | 0.009428 | 0.105 | |

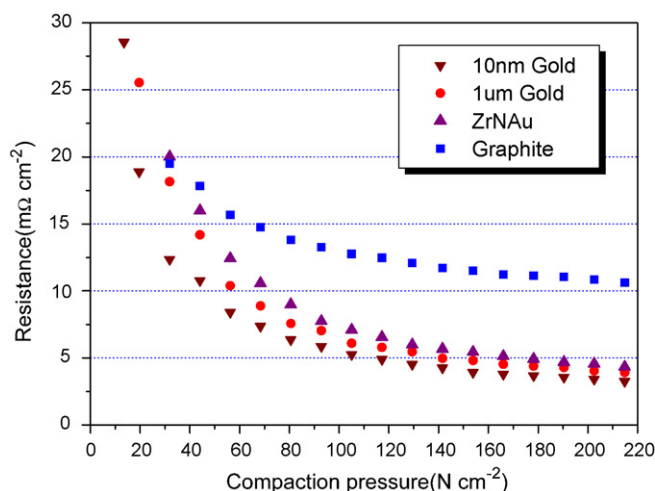


Fig. 15. Contact resistance results of 10 nm, 1 μm, ZrNAu-coated samples and graphite plate.

3.2. Contact resistance measurements

For comparison, the contact resistance of a typical graphite plate was measured. It can be seen that 10 nm gold samples exhibited the lowest contact resistance among the candidates as summarized in Fig. 15. The ZrNAu samples show similar low contact resistance to that of the 10 nm gold; this is simply because the gold layer of 10 nm thickness in ZrNAu is coated on top of the ZrN coating. Comparing with 2 nm, 10 nm, and 1 micron gold samples, the 2 nm gold coating (Fig. 16) reduces the contact resistance of a bare 316 material to about one third.

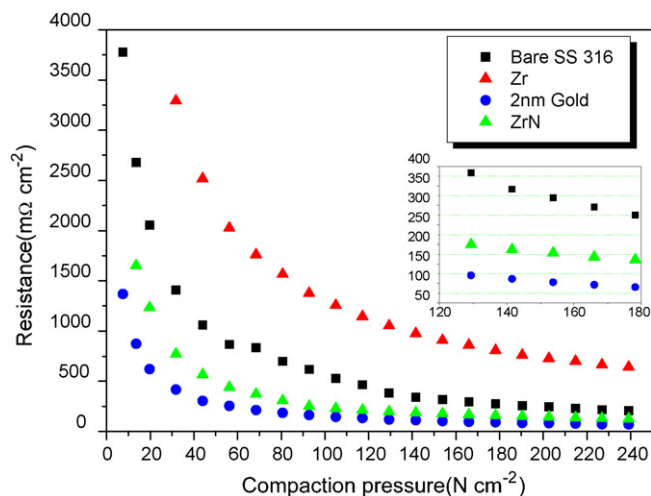


Fig. 16. Contact resistance results of bare SS 316, Zr, ZrN, and 2 nm gold-coated samples.

Also, there is no perceptible difference in the contact resistance between 10 nm and 1 μm gold coating; small difference between the two results in Fig. 15 could be due to noises/error in the measurement, sample condition or other factors. This fact implies that there exists a thinnest thickness of gold to meet the requirement. In Fig. 16, the contact resistance of the ZrN sample is significantly lower than the pure Zr-coated sample and even lower than bare SS 316. The Zr-coated sample shows the best corrosion resistance among the coated samples without gold coating, but it cannot be considered as a viable coating for potential bipolar plate due to the high contact resistance.

4. Summary and conclusions

Short-term polarization and contact resistance tests have been performed for a set of coating materials and substrates. Corrosion potential and corrosion current are extrapolated from the polarization test results for each sample and they are used to rank the corrosion resistance of the coated metallic bipolar plate materials. The more positive the corrosion potential and the smaller the corrosion current, the more corrosion resistant are the coated metallic samples. The Zr, ZrN, ZrNb, ZrNAu and 10 nm gold-coated samples satisfied the DOE target at the typical anode potential of PEMFC, but only the Zr-coated sample satisfied the DOE goal at the typical cathode potential. Gold-coated samples such as ZrNAu and 10 nm gold met the DOE target for contact resistance. Also, the nitrated surface showed better surface conductivity than the original metal. In terms of gold thickness effect, the thicker the gold coating, the better the interfacial electrical conductivity and the corrosion resistance. However, there is a minimum thickness of gold for satisfying the contact resistance goal. The 10 nm gold coating renders adequate corrosion resistance for the anode side of the bipolar plate, but it is not thick enough to protect the metal from corrosion at the cathode side. For future work, polarization tests will be performed for more coating candidates; long-term corrosion and actual fuel cell testing will be carried out to further investigate the endurance of selected coated metallic bipolar plates.

Acknowledgement

The authors would like to thank Dr. Kirk Weisbrod with Los Alamos National Laboratory for helpful discussions.

References

- [1] H. Tawfik, Y. Hung, D. Mahajan, J. Power Sources 163 (2007) 755.
- [2] S.-J. Lee, C.-H. Huang, J.-J. Lai, Y.-P. Chen, J. Power Sources 131 (2004) 162.

- [3] P.R. Roberge, Handbook of Corrosion Engineering, McGraw-Hill, pp. 2000, in press.
- [4] <<http://www.corrosion-doctors.org/InternetResources/NPL.htm#Electrochemistry>>.
- [5] <http://www.gamry.com/App_Notes/DC_Corrosion/GettingStartedWithEchemCorrMeasurements.htm>.
- [6] R. Hornung, G. Kappelt, J. Power Sources 72 (1998) 20.
- [7] J.A. Turner, H. Wang, in: DOE Annual Progress Report, 2005.
- [8] E. Fleury, J. Jayaraj, C.H. Kim, H.K. Seok, K.Y. Kim, J.B. Kim, J. Power Sources 159 (2006) 34.
- [9] R.C. Makkus, A.H.H. Janssen, F.A. Bruijn, R. Mallant, J. Power Sources 86 (2000) 274.
- [10] D.P. Davies, P.L. Adcock, M. Turpin, S.J. Rowen, J. Power Sources 86 (2000) 237.
- [11] M.C. Li, C.L. Zeng, S.Z. Luo, J.N. Shen, H.C. Lin, C.N. Cao, Electrochim. Acta 48 (2003) 1735.
- [12] P.L. Hentall, J.B. Lakeman, G.O. Mepsted, P.L. Adcock, J.M. Moore, J. Power Sources 80 (1999) 235.
- [13] A.S. Woodman, E.B. Anderson, K.D. Jayne, M.C. Kimble, Am. Electroplaters Surf. Finish. Soc. (1999) 1735.
- [14] S.-H. Wang, J. Peng, W.-B. Lui, J.-S. Zhang, J. Power Sources 162 (2006) 486.
- [15] M.P. Brady, K. Weisbrod, I. Paulauskas, R.A. Buchanan, K.L. More, H. Wang, M. Wilson, F. Garzon, L.R. Walker, Scripta Mater. 50 (2004) 1017.
- [16] H. Wang, M.P. Brady, K.L. More, H.M. Meyer, J.A. Turner, J. Power Sources 138 (2004) 79.
- [17] R. Tian, J. Sun, L. Wang, Int. J. Hydrogen Energy 31 (2006) 1874.
- [18] M. Li, S. Luo, C. Zeng, J. Shen, H. Lin, C.N. Cao, Corros. Sci. 46 (2004) 1369.
- [19] E.A. Cho, U.S. Jeon, S.A. Hong, I.H. Oh, S.G. Kang, J. Power Sources 142 (2005) 177.
- [20] H. Wang, M.A. Sweikart, J.A. Turner, J. Power Sources 115 (2003) 243.
- [21] H. Wang, G. Teeter, J.A. Turner, J. Electrochem. Soc. 152 (2005) B99.
- [22] K. Banerjee, A. Amerasekera, G. Dixit, C. Hu, Proceedings of the Electron Devices Meeting, IEEE, Washington, DC, 1997, p. 115.
- [23] Keithley, Low Level Measurements; Precision DC Current, Voltage, and Resistance Measurements, User Manual (2004) 4–26.
- [24] Y. Wang, D.O. Northwood, Electrochim. Acta 52 (2007) 6793.